Self-assembled porphyrin–peptide cages for photodynamic therapy

Chandramouli Ghosh, Lamiaa Ali, Yannick Bessin, Sébastien Clément, Sébastien Richeter, Nadir Bettache, Sébastien Ulrich

FULL PAPER

Self-Assembled Porphyrin-Peptide Cages for Photodynamic Therapy

Chandramouli Ghosh,[a,†] Lamiaa M. A. Ali,[a,b†] Yannick Bessin,[a] Sébastien Clément,[c] Sébastien Richeter,[c*] Nadir Bettache,[a*] and Sébastien Ulrich[a*]

Received 00th January 20xx,
Accepted 00th January 20xx

DOI: 10.1039/x0xx00000x

The development of photodynamic therapy requires access to smart photosensitizers which combine appropriate photophysical and biological properties. Interestingly, supramolecular and dynamic covalent chemistries have recently shown their ability to produce novel architectures and responsive systems through simple self-assembly approaches. Herein, we report the straightforward formation of porphyrin-peptide conjugates and cage compounds which feature on their surface chemical groups promoting cell uptake and specific organelle targeting. We show that they self-assemble, in aqueous media, into positively-charged nanoparticles which generate singlet oxygen upon green light irradiation, while also undergoing a chemically-controlled disassembly due to the presence of reversible covalent linkages. Finally, the biological evaluation in cells revealed that they act as effective photosensitizers and promote synergistic effects in combination with Doxorubicin.

Introduction

PhotoDynamic Therapy (PDT) is an approved clinical modality used to treat various diseases such as cancer, age-related macular degeneration, and skin lesions.[1-5] PDT operates through the action of light that excites a photosensitizer which then produces short-lived cytotoxic Reactive Oxygen Species (ROS, type I PDT) or singlet oxygen ($^1O_2$, type II PDT), leading to local cell death through conventional and non-conventional cell death programs, activation of immune cells or vascular damage.[6, 7] An ideal photosensitizer is therefore non-toxic in dark but becomes cytotoxic when irradiated with light at the appropriate wavelength. Porphyrins and their derivatives form a well-known class of photosensitizers (*e.g.* approved porphyrin-based photosensitizers: Photofrin®, Visudyne®) which displays an efficient light absorption (absorption Soret band around 400 nm and Q bands at 500-700 nm) and high singlet oxygen quantum yields.[8] While the design of photosensitizers absorbing low-energy light in the therapeutic window (650 nm – 1100 nm)[9, 10] has seen major advances,[11] their polyaromatic structure often make them poorly soluble in aqueous media, and this is certainly true for porphyrin-based photosensitizers. Their aggregation can alter their photophysical properties, either by turning the inter-system crossing and ROS/$^1O_2$ production "on" in presence of J-aggregates,[12, 13] or "off" in the presence of H-aggregates,[14] depending on the molecular structure of the photosensitizers and on the supramolecular organization of the aggregates.[15, 16] The conjugation to biomolecules such as peptides or carbohydrates can therefore be of interest to improve solubility, but also to position functional groups that improve cell internalization[17, 18] and may promote targeted delivery.[19-25] PDT has indeed a local effect due to the limited diffusion of ROS/$^1O_2$ (10 nm – 2 µm)[26-28] which potency depends on the precise subcellular localization of the photosensitizer. Peptides are water-soluble and biocompatible building blocks which are interesting in this regard due to i) their ability to engage in β-sheets formation and thus direct the precise self-assembly of porphyrin-based photosensitizers, ii) the sensitivity of their assemblies to pH or enzymes, and iii) their cell-penetrating and targeting features.[29-31] In order to achieve multivalent binding and stabilization, it is necessary to graft multiple peptides onto porphyrin-based photosensitizers. However, most of the reported porphyrin-peptide conjugates bear only one or two peptides,[11] and the synthetic methodology for obtaining tetra-conjugates still remains a current challenge.[32]

Supramolecular chemistry has recently been implemented in the context of PDT where it can contribute to i) improving solubility/delivery using host-guest systems,[33-37] or ii) accessing smart nano-assemblies of photosensitizers, such as metallacages,[38, 39] Covalent-Organic Frameworks (COFs),[40] nanovesicles,[41] and other self-assembled nanomaterials[29, 42, 43] which display unique photophysical and/or biological features. Dynamic covalent chemistry combines the attractive features of dynamic self-assembly of supramolecular systems and add the

[a] *Institut des Biomolécules Max Mousseron (IBMM), Université of Montpellier, CNRS, ENSCM, Montpellier, France.*
[b] *Department of Biochemistry Medical Research Institute, University of Alexandria, 21561 Alexandria, Egypt.*
[c] *Institut Charles Gerhardt Montpellier (ICGM), Université de Montpellier, CNRS, ENSCM, Montpellier, France.*
† These authors contributed equally to this work.

Electronic Supplementary Information (ESI) available: [Synthetic details, ^1H, 2D, and DOSY NMR, HPLC and mass spectrometry characterization data of all peptides, TPP conjugates and cages, UV-Vis absorption and fluorescence analyses, complementary data on singlet oxygen generation and PDT on cells]. See DOI: 10.1039/x0xx00000x

enticing perspective of obtaining covalent assemblies of high stability in biological media, yet with sensitivity to reactional cues that may be exploited in delivery applications.[44, 45] As a recent representative example of an innovative strategy using dynamic covalent chemistry for the discovery of new bioactive compounds, Anslyn and co-workers reported the access to quaternary assemblies of peptides, which proved to be effective antibiotics.[46] Another recent work revealed the ability of organic cage-type compounds, obtained through dynamic covalent synthesis, to readily cross cell membranes and enter cells.[47] In this work, we explored a dynamic covalent chemistry approach for the formation of porphyrin-peptide conjugates. We report the straightforward access to four cationic tetra-conjugates and eight cage-type structures displaying cell-penetrating and targeting groups. We show their self-assembly in aqueous media into positively-charged nanoparticles, their chemically-controlled disassembly, evidence their propensity to generate singlet oxygen upon green light irradiation, and demonstrate their action as effective photosensitizers in live cells.

Results and discussion

Design.

Our design uses porphyrin tetra-aldehyde **TPP-Ald** and **Zn-TPP-Ald** as known photosensitizer cores[48, 49] onto which C-hydrazide peptides can be appended through acylhydrazone condensation reactions (Scheme 1). The choice of inserting zinc(II) within the porphyrin was dictated by previous reports showing that it maintains the photophysical properties while improving cell uptake through direct interactions with the phospholipids of cell membranes.[50] Peptide possessing a *L*-cysteine were selected as a novel entry to access porphyrin cage compounds[51] through DMSO-promoted disulphide formation,[52-54] while the peptide with the isostructural *L*-serine amino acid led to tetra-conjugate compounds (Scheme 1). These disulphide-bridged cages were also considered in view of their potential to perform thiol-mediated uptake.[55, 56] The N-termini were selected in order to display i) cationic groups that favor cell uptake, such as *L*-arginines as in cell-penetrating peptides (**TPP-Arg$_4$**, **TPP-Arg$_8$**, **Zn-TPP-Arg$_4$**, **Zn-TPP-Arg$_8$**, **CAGE-Arg**, and **Zn-CAGE-Arg**; **CAGE-H** and **Zn-CAGE-H** serving as a neutral references),[57, 58] ii) boronic acid for promoting cell uptake and lysosome escape (**CAGE-BA** and **Zn-CAGE-BA**),[59-62] and iii) triphenylphosphonium for mitochondria targeting (**CAGE-PPh$_3$** and **Zn-CAGE-PPh$_3$**).[21, 63-65]

Synthesis and characterizations.

TPP-Ald was synthesized as previously described,[66] and its metalation afforded **Zn-TPP-Ald** (ESI, Figures S1-2). The peptide hydrazides were synthesized through a solid phase peptide synthesis (SPPS) approach using a modified resin (ESI, Scheme S1, Figures S3-26). Finally, the coupling of the porphyrin tetra-aldehyde cores with the peptide hydrazides was carried out by adapting related protocols, mixing stoichiometric quantities at a final concentration of **TPP-Ald** of 2 mM favouring discrete cage compounds in DMSO/H_2O 94/6 and heating up at 50 °C for 2 days.[52-54] ^{1}H NMR indicated the disappearance of the aldehyde peak (Figure S27). Completion of the reactions was confirmed by HPLC[67] while the ESI-MS or MALDI-ToF analyses indicated the formation of the expected TPP tetra-conjugates or TPP cages (Figure 1 and Figures S28-38). Similarly, DOSY NMR revealed an increase in hydrodynamic radii when converting the starting **TPP-Ald** and **Zn-TPP-Ald** into the tetra-conjugates and cage compounds (Table S1 and Figure S39). Further characterization by UV-Vis absorption and fluorescence spectroscopies revealed that, in DMSO, the tetra-conjugate preserve similar spectroscopic properties compared to the parent **TPP-Ald** and **Zn-TPP-Ald**, while the cage compounds have a lower fluorescence intensity most likely arising from aggregation-caused quenching (ACQ) due to the proximity of the two porphyrin cores (Figure S40). The situation is slightly different in H_2O as all tetra-conjugate and cage compounds now display more intense electronic absorption and fluorescence, most likely due to an improved water-solubility compared to the parent **TPP-Ald** and **Zn-TPP-Ald** thanks to the presence of the hydrophilic peptides (Figure S41).

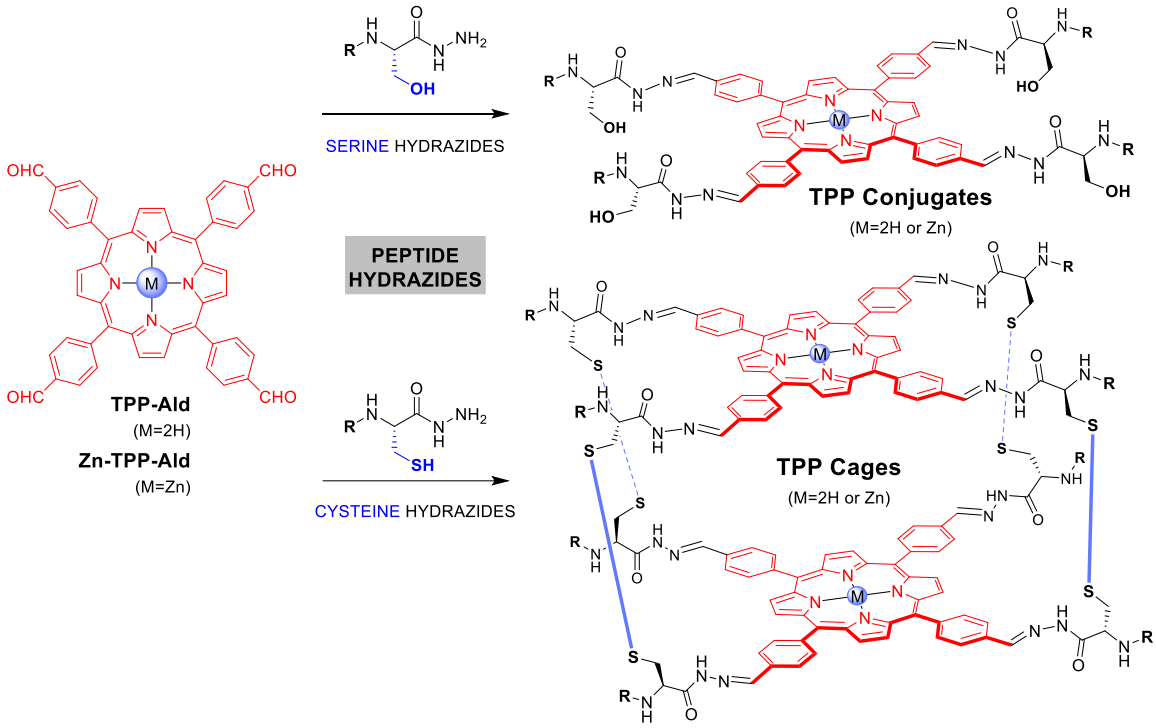

R	Serine Hydrazides	Cysteine Hydrazides	TPP Conjugates M = 2H	TPP Conjugates M = Zn	TPP Cages M = 2H	TPP Cages M = Zn
H	/	CysHyd	/	/	CAGE-H	Zn-CAGE-H
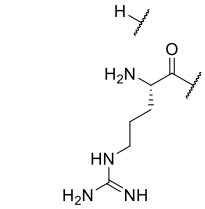	ArgSerHyd	ArgCysHyd	TPP-Arg$_4$	Zn-TPP-Arg$_4$	CAGE-Arg	Zn-CAGE-Arg
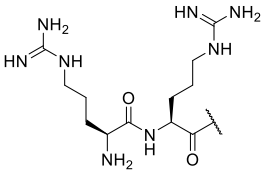	Arg$_2$SerHyd	/	TPP-Arg$_8$	Zn-TPP-Arg$_8$	/	/
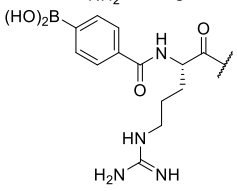	/	BA-ArgCysHyd	/	/	CAGE-BA	Zn-CAGE-BA
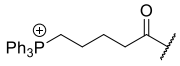	/	PPh$_3$CysHyd	/	/	CAGE-PPh$_3$	Zn-CAGE-PPh$_3$

Scheme 1. Chemical structures of porphyrin and peptide building blocks, and synthetic route toward TPP tetra-conjugates and TPP Cages by one-pot simultaneous acylhydrazone and disulphide formations.

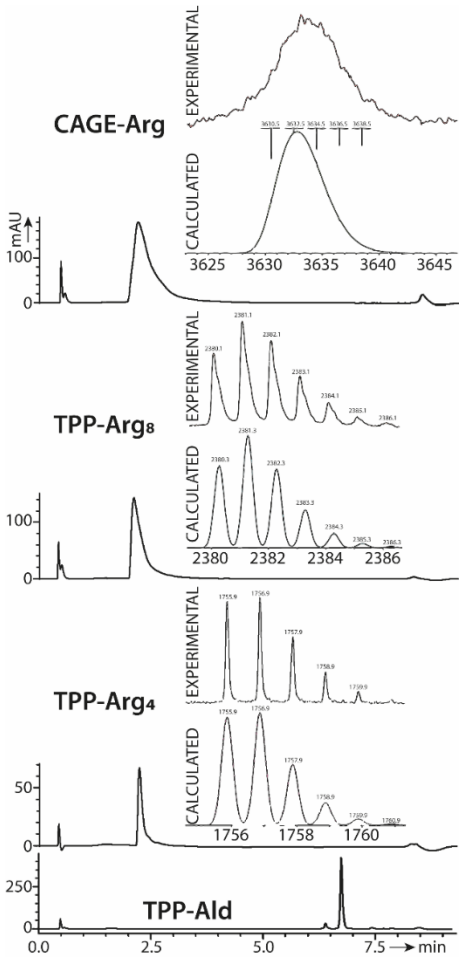

Figure 1. HPLC chromatograms and MALDI-ToF mass spectrometry analyses of, from bottom to top, **TPP-Ald**, **TPP-Arg4**, **TPP-Arg8**, and **CAGE-Arg**.

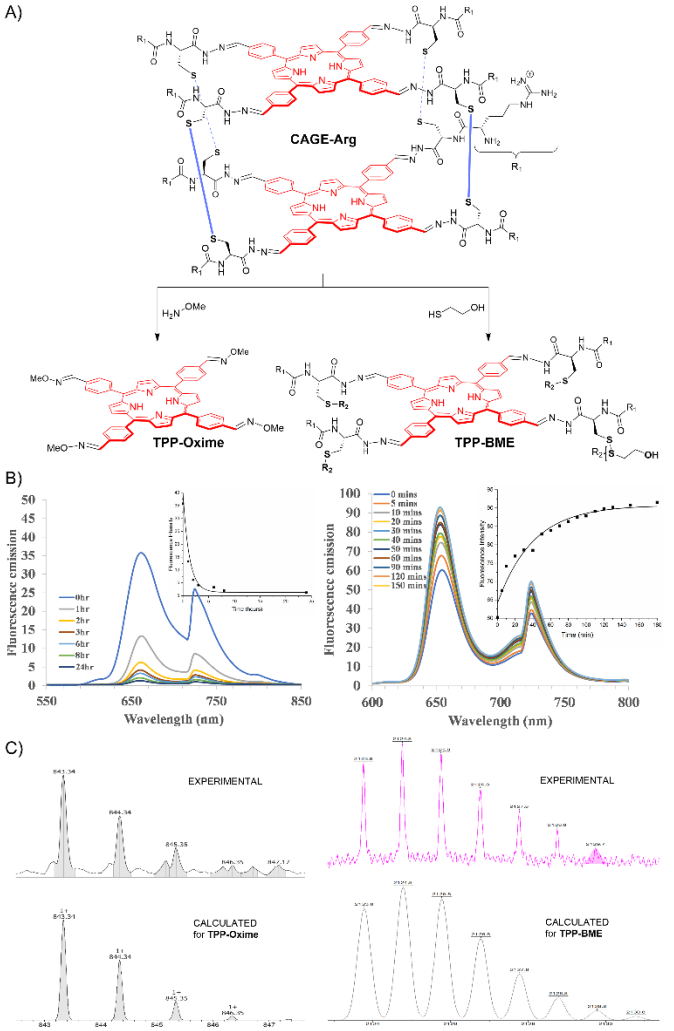

Figure 2. A) Chemically-controlled degradation of **CAGE-Arg** upon addition of methoxyamine or β-mercaptoethanol, leading to the formation of **TPP-Oxime** and **TPP-BME**, respectively; B) monitoring of the degradation processes by fluorescence spectroscopy (λ_{exc} = 420 nm; insets showing the time evolution of fluorescence emission intensity at λ_{em} = 655 nm); C) analyses by MALDI-ToF of the end-products formed after, respectively, 24 and 3 hours.

Chemically-controlled degradation.

Since the TPP tetra-conjugates and TPP cages are made of responsive covalent linkages, namely acylhydrazones and disulphides, we probed their controlled degradation by monitoring the fluorescence emission of **CAGE-Arg** (Figure 2A) in DMSO. The data show a decrease in fluorescence emission in presence of methoxyamine ($t_{½}$ ~ 1 hour), and an increase in presence of β-mercaptoethanol ($t_{½}$ ~ 20 min) (Figure 2B). Confirmation of the covalent exchange reactions was obtained by mass spectrometry analyses which confirm the formation of **TPP-Oxime** and **TPP-BME** (Figure 2C).

Self-assembly in aqueous media and singlet oxygen generation.

Dynamic Light Scattering and ζ potential measurements were carried out and showed nanoparticles formation in phosphate buffer at pH 7.0 (Table 1). Similar positively-charged nanoparticles were obtained for both **TPP-Arg4** and **CAGE-Arg** compounds, while the zinc(II) counterparts gave smaller nanoparticles, in line with the DOSY NMR results.

Table 1. Dynamic light scattering and ζ-potential results measured in 0.1 M phosphate buffer (pH 7.0) solutions.

Compound	Size ± SD (nm)	PDI ± SD	ζ-potential ± SD (mV)
CAGE-Arg	257.8 ± 14.5	0.430 ± 0.017	+15.3 ± 2.8
TPP-Arg$_4$	212.7 ± 3.5	0.334 ± 0.092	+10.3 ± 0.9
Zn-CAGE-Arg	182.9 ± 15.6	0.392 ± 0.034	+14.8 ± 2.3
Zn-TPP-Arg$_4$	105.8 ± 16.7	0.670 ± 0.032	+12.4 ± 1.0

The ability of TPP tetra-conjugates and TPP cages to produce singlet oxygen ($^1O_2$) upon green light irradiation (λ_{exc} = 525 nm) was probed, in aqueous media (0.1 M phosphate buffer, pH 7.0) and relative to a positive control (*meso* 5,10,15,20-tetrakis(N-methylpyridinium-4-yl)porphyrin iodide, H_2TMPyP),[68] by UV absorption spectroscopy using 9,10-anthracenediyl-bis(methylene)dimalonic acid (ABDA) as a selective $^1O_2$ sensor.[29, 69] ABDA and $^1O_2$ react through a [4 + 2] cycloaddition, resulting in the formation of the corresponding 9,10-endoperoxide. Therefore, $^1O_2$ generation can be proved by monitoring the decrease of the absorption at λ = 379 nm. The plots of ln(A_0/A) measured at λ = 379 nm show linear increases with the irradiation time and confirm the key role of the photosensitizers in the observed $^1O_2$ production (Figures 3 and S42). All tested compounds are found better photosensitizers than H_2TMPyP. Interestingly, the cage compounds **CAGE-H**, **CAGE-Arg**, and **Zn-CAGE-Arg** were found superior to the tested tetra-conjugates **TPP-Arg$_4$** and **Zn-TPP-Arg$_4$**.

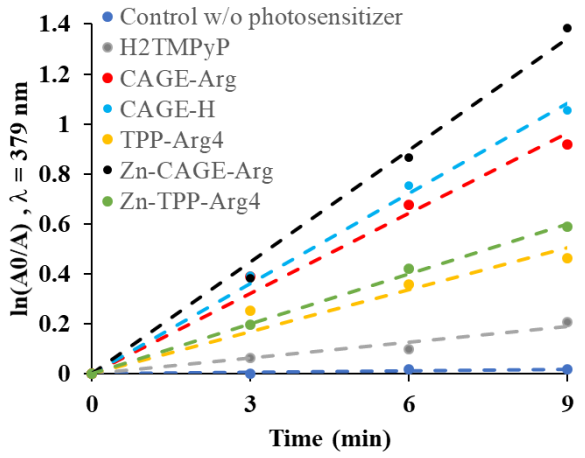

Figure 3. Singlet oxygen generation of TPP tetra-conjugates and TPP cages derivatives (all at a final constant concentration of TPP of 1 µM) in water, probed by UV absorption spectroscopy (absorbance measured at 379 nm) using ABDA (100 µM) at varying light irradiation times (green light, λ = 525 nm). Negative control experiment was performed without photosensitizer.

Cytotoxicity.

Cytotoxicity was measured on human breast cancer MCF-7 cells using a MTT assay (Figure 4). The results show that **CAGE-H**, **CAGE-BA**, and **CAGE-PPh$_3$** are essentially non-toxic up to a 10 µM dose, while the cationic **CAGE-Arg**, **TPP-Arg$_4$**, and **TPP-Arg$_8$** do show a gradual decrease in cell viability when increasing the dose. It is however interesting to note that **CAGE-Arg** is significantly less cytotoxic than **TPP-Arg$_8$** even though both of them present the same number of cationic *L*-arginines, suggesting a different mode of interaction with cells. The zinc-containing derivatives show a similar trend but cytotoxicity becomes more pronounced at high dose (20 µM).

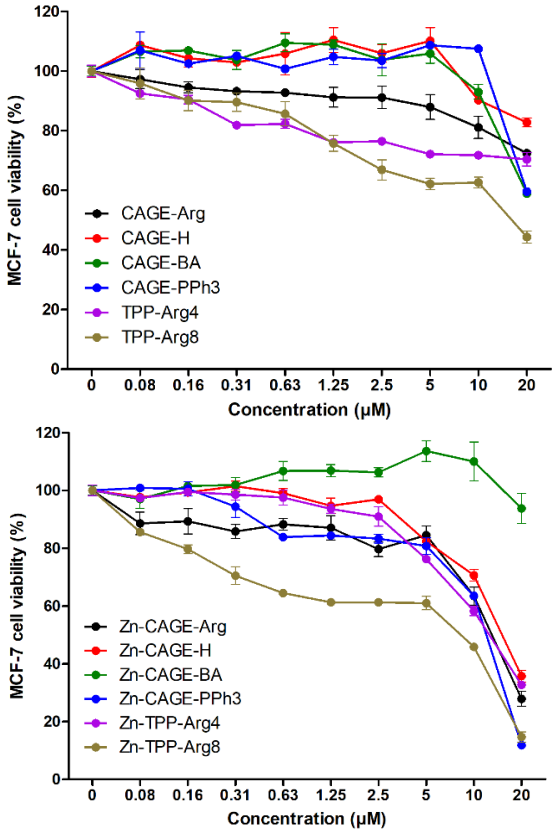

Figure 4. Cytotoxicity study in human breast cancer (MCF-7) cells after 3 days of incubation with different concentrations of TPP derivatives (top: free base porphyrin compounds; bottom: zinc porphyrin complexes). Data are presented as mean ± SEM.

PDT on cells.

The PDT effect on human breast cancer MCF-7 cells was determined by measuring cell viability by MTT assays under dark conditions and after light irradiation (Figure 5). Although near-IR light has deeper tissue penetration, we selected here green light because it matches the Q-bands absorption of our porphyrin cages. A concentration of 1.31 µM was used as both cell viability in dark conditions and singlet oxygen generation were optimum at this dose for all TPP derivatives. While the neutral **CAGE-H** was ineffective, the cationic **CAGE-Arg** showed a significant effect which depends upon the light irradiation time. A similar effect was observed for **CAGE-BA** and **CAGE-PPh$_3$**, with a potency that matches that of **TPP-Arg$_4$** and **TPP-Arg$_8$**. Increasing the incubation time from 3 hours to 24 hours did not change this trend (Figure S43). Unfortunately, expect for **Zn-CAGE-Arg**, the zinc-containing series of TPP derivatives did not show good PDT activity despite effective singlet oxygen generation (Figure S43).

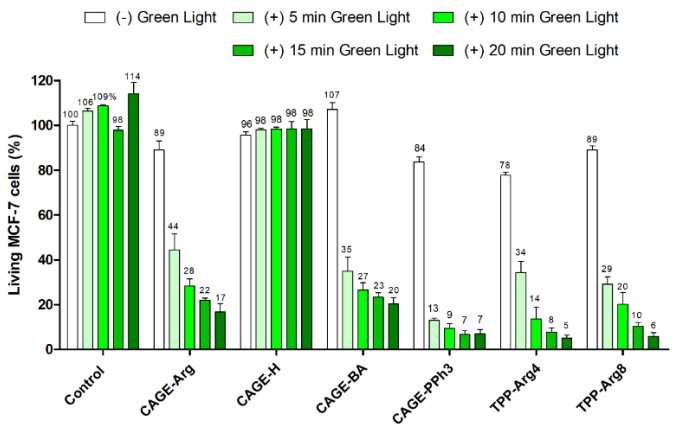

Figure 5. PDT study in human breast cancer (MCF-7) cells incubated with 1.31 µM of compounds for 3 h then exposed to green light for different irradiation times. Data are presented as mean ±SEM.

The evidence that the decrease in cell viability upon light irradiation is indeed due to the photosensitizer-induced generation of reactive oxygen species (ROS) was obtained from in-cell imaging studies, which showed intracellular ROS production only in the presence of **CAGE-Arg** *and* green light irradiation (Figure 6). Furthermore, the magnitude of ROS production correlates well with the PDT activity of the tested compounds, for instance the PDT-inactive **CAGE-H** showing weak intracellular ROS production (Figure S44).

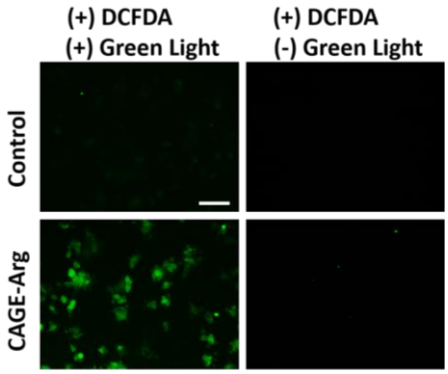

Figure 6. Fluorescence microscopy imaging of ROS using DCFDA assay in human breast cancer (MCF-7) cells treated (or not) with 1.31 µM of cage for 24 h, then, exposed (or not) to green light irradiation for 2 min. Scale bar 100 µm.

Cell internalization.

The kinetic of cell uptake was determined by fluorescence activated cell sorting. The cationic **CAGE-Arg** was found to internalize faster, and more rapidly than **TPP-Arg$_4$** and **TPP-Arg$_8$** (Figure 7). The fact that **CAGE-H** gave positive results while it showed no PDT activity and weak ROS production points out to a poor singlet oxygen quantum yield in the intracellular environment, in contradiction to what was found in aqueous media (Figure 3). In the zinc-containing series, **Zn-CAGE-Arg** was also internalized faster than **Zn-TPP-Arg$_4$** according to FACS analysis (Figure S45).

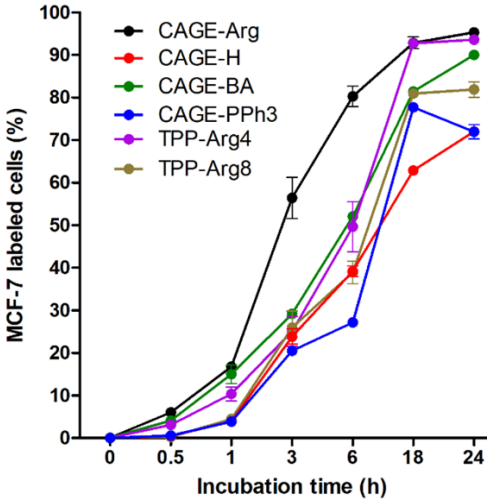

Figure 7. Uptake kinetics study of compounds incubated with human breast cancer (MCF-7) cells at 1.31 µM concentration for different time intervals. Data are presented as mean ± SEM.

The study was completed by confocal fluorescence imaging studies which unambiguously showed the more effective cell internalization of **Cage-Arg** compared to **TPP-Arg$_4$** (Figure 8).

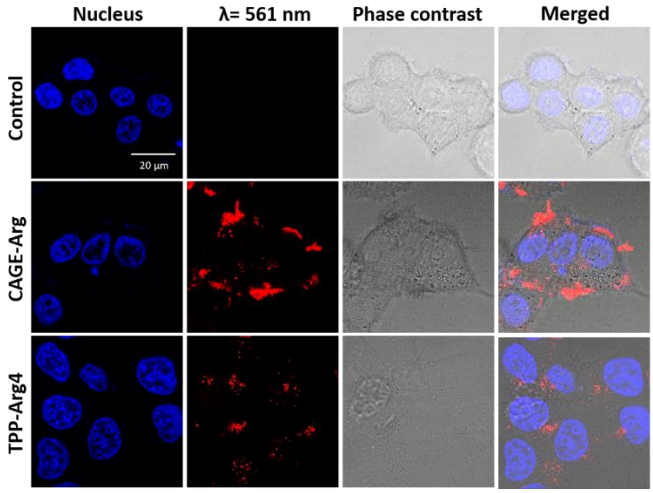

Figure 8. Confocal microscopy imaging of live human breast cancer (MCF-7) cells treated with 2.62 µM of **Cage-Arg** or **TPP-Arg$_4$** for 24 h. Images were acquired using objective 63x (Zoom 2).

We probed the mechanism of cell penetration by quantifying the cell uptake by FACS in the presence of different inhibitors of internalization pathways: methyl-β-cyclodextrin (MβCD) suppressing cholesterol-dependent clathrin independent endocytosis involving lipid rafts, chlorpromazine hydrochloride (CPZ) suppressing clathrin-dependent endocytosis, 5-(N,N-dimethyl)amiloride hydrochloride (DMA) suppressing micropinocytosis, and Ellman's reagent (5,5-dithio-bis-(2-nitrobenzoic acid), DTNB) suppressing thiol-mediated uptake.[70] The results reveal that clathrin-dependent endocytosis is the main route of cell internalization followed by caveolae-mediated endocytosis – micropinocytosis and thiol-mediated uptake not being used (Figure 9). This is in contrast with neutral

organic cages which were shown to enter cell through passive diffusion.[47]

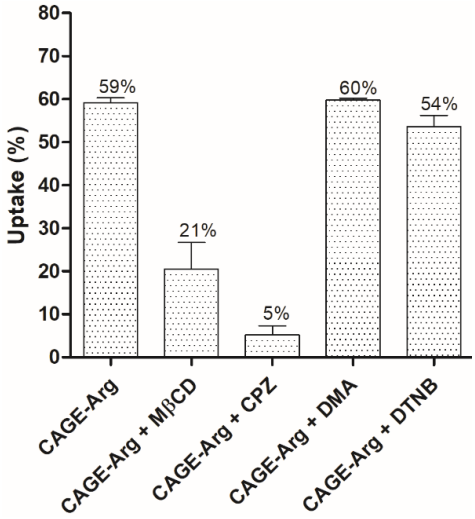

Figure 9. Endocytosis mechanism study using cell internalization inhibitors (methyl-β-cyclodextrin (MβCD, 5 mM), chlorpromazine hydrochloride (CPZ, 50 µM), 5-(N,N-dimethyl)amiloride hydrochloride (DMA, 40 µM), and 5,5-dithio-bis-(2-nitrobenzoic acid) (DTNB, 1.2 mM)) incubated with 1.31 µM **CAGE-Arg** for 3 h in human breast cancer (MCF-7) cells. Data are presented as mean ± SEM.

Dual therapy.

Cage compounds can have the ability to encapsulate a guest of interest (e.g. fluorophore, drug) and transport it inside cells. The PDT action can also potentiate and permeabilize cell and endosome membranes, resulting in the subsequent cell uptake and delivery of drugs in the cytosol[71] through a process called photochemical internalization (PCI).[72, 73] Reasoning that aromatic guests could possibly bind within the TPP cages through π-π interactions, we then studied the combination of our TPP photosensitizers with the aromatic cytotoxic anticancer drug Doxorubicin (Figure 10). In the absence of light irradiation, no reduction in cell viability on human breast cancer (MCF-7) cells was observed, also for Doxorubicin alone at a dose of 0.65 µM below its reported IC_{50} of 1.9-2.5 µM.[74, 75] Light irradiation had no effect on cells incubated with Doxorubicin alone but triggered a strong PDT effect on cells incubated within combinations of TPP tetra-conjugates/cages with Doxorubicin. The unexpected result is that the activity of the combination **CAGE-Arg** and Doxorubicin is more potent than **CAGE-Arg** or Doxorubicin alone, the calculated combination index (CI) value of 0.06 revealing a synergistic effect where **CAGE-Arg** potentiates the action of Doxorubicin. Although we had hoped that this effect can be directed by host-guest recognition of Doxorubicin with the hydrophobic cavity of **CAGE-Arg**, the fact that this potentiating effect was also observed with **TPP-Arg$_4$** rules out this possibility and rather suggest a PCI mechanism.

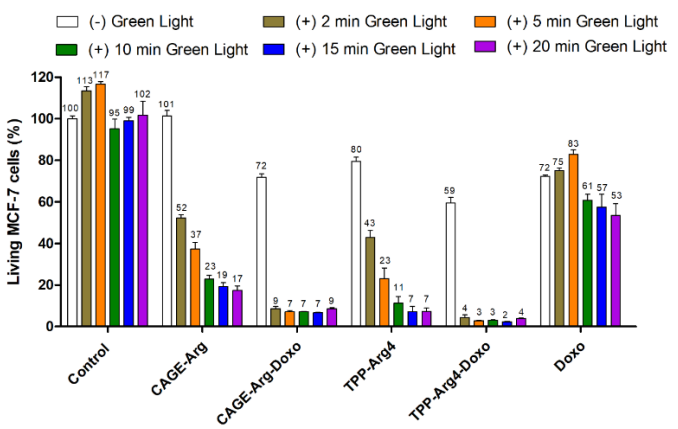

Figure 10. PDT study in human breast cancer (MCF-7) cells incubated with 1.31 µM of TPP derivatives alone or combined with doxorubicin, and free doxorubicin (0.65 µM) for 3 h then exposed to green light for different irradiation times. Data are presented as mean ± SEM.

Experimental section

All reagents and solvents were obtained from commercial sources and were used without further purification. *Meso* tetra(p-formylphenyl)porphyrin (**TPP-Ald**) was synthesized as previously described.[66]

Nuclear Magnetic Resonance (NMR). ^{1}H and DOSY NMR experiments were measured at room temperature in deuterated solvents with a Bruker Avance 400 instrument at 400 MHz. Peaks were referenced in ppm with respect to the residual solvent peak (CD_3OD: δ = 3.31 ppm; D_2O: δ = 4.79 ppm). Data are reported as follows: chemical shift (δ in ppm), multiplicity (s for singlet, d for doublet, dd for doublet of doublet, t for triplet, dt for doublet of triplet, m for multiplet, br for broad signal), coupling constant (*J* in Hertz) and integration. DOSY NMR were carried out in DMSO (dynamic viscosity 1.996 mPa.S used for the Stockes-Einstein equation).

High-performance liquid chromatography (HPLC). Analytical reverse-phase HPLC (RP-HPLC) analyses were performed on a Thermo Scientific HPLC Dionex Ultimate 3000 (Phenomex Kenetex C18, 2.6 µm x 7.5 cm, 100 Å) with the following linear gradients of solvent B (99.9% acetonitrile, 0.1% TFA) into solvent A (99.9% H2O, 0.1% TFA): Method: 5 to 100% of solvent B in 5 min; flow: 1 mL/min. Preparative HPLC was performed on i) a Gilson PLC2250 Prep (XSelect CSH Prep C18, 5 µm, 250 x 30 mm column, Waters) , flow 40 mL/min, or on ii) a VWR International LaPrep pump P110, a VWR LaPrep P314 Dual l absorbance detector and EZChrom software (15 C18 reversedphase column Waters x-bridge, RP-18, 250 x 25 mm, 5 µm), flow 40 mL/min, using linear gradients of eluents A (99.9% H2O, 0.1% TFA) and B (99.9% acetonitrile, 0.1% TFA).

Liquid chromatography-mass spectrometry (LC/MS). Analyses were performed on a Shimadzu LCMS2020 (Phenomex Kinetex C18, 2.6 µm x 7.5 cm, 100 Å) equipped with a SPD-M20A detector with the following linear gradient of solvent B (99.9% acetonitrile, 0.1% HCOOH) and solvent A (99.9% H_2O, 0.1% HCOOH): 5 to 95% of solvent B in 5 min; flow 1 mL/min. Retention times (t_R) are given in minutes.

Mass spectrometry (MS). Electrospray ionization (ESI-MS) and MALDI-ToF (matrix: sinapic acid) analyses were carried out at the Plateforme d'Analyse et de Caractérisation (PAC) of the Pôle Chimie, Université de Montpellier using Micromass Q-Tof instruments.

General procedure of Fmoc hydrazine modified 2-chlorotrityl resin. Following a previous report,[76] 2-chlorotrityl chloride resin (CTC, loading 1.6 mmol/g) (2 g) was swollen in CH_2Cl_2 (16 mL) at 0 °C. Fmoc hydrazine hydrochloride (1.627g, 2 eq.) and diisopropylethylamine (3.1 mL, 10 eq.) were dissolved in DMF (20 mL) and CH_2Cl_2 (4 mL). The above solution was then added dropwise into the resin slurry at 0 °C. The reaction mixture was gently stirred from 0 °C to room temperature overnight. Methanol (0.32 mL) was added to quench the remaining 2-CTC resin. The resulting resin was washed with DMF (35 mL), H_2O (35 mL), DMF (35 mL), methanol (35 mL), diethyl ether (35 mL) and kept under high vacuum for 2 h. The dried Fmoc hydrazine 2-CTC resin was purged with nitrogen and stored at 4°C. The loading of resin was quantified by UV-visible absorption spectroscopy as follows: 10 mg of resin was suspended in 1 mL of piperidine/DMF (2:8) for 30 mins. After filtration, 100 µL of the filtrate was diluted in 9.9 mL of DMF. Then, the absorbance was measured at 301 nm and the loading of the modified resin was determined by the equation $Loading = \text{Absorbance x } 10^4/7800$.

General procedure of Solid-Phase Peptide Synthesis (SPPS). The syntheses of peptides was based on a Fmoc strategy and was carried out manually, by adapting previous protocols,[52, 76] using the following conditions:

-Resin deprotection (Fmoc removal): piperidine/DMF (2/8) at r.t. for 5 min, twice;

-Coupling conditions: Fmoc-AA-OH (0.6 M, 3 eq.), HATU (0.2 M, 3 eq.), DIEA (6 eq.), DMF, stirred at r.t. for 30 min (double coupling, 30 min);

-Fmoc deprotection conditions: 10 mL of piperidine/DMF (2/8) at r.t. for 5 min, twice;

-Mild cleavage conditions (10 mL of TFA/CH_2Cl_2 1/99 for 5 min, 4 times, followed by addition of 20 mL MeOH/Pyridine 8/2) and purification by preparative reverse-phase HPLC;

-Full deprotection: TFA/TIS/H_2O 95/2.5/2.5 at r.t. for 12 h, then precipitation in Et_2O.

The final peptides were titrated by ^1H NMR (D_2O) using *tert*-butanol as internal reference in order to determine their exact molar concentration. For this, the compound was solubilized in D_2O (final concentration around 5 mM) and *tert*-butanol was added (25 µL, 13.3 mM) in the NMR tube (total volume of 600 µL). ^1H NMR spectrum was recorded and the relative peak integration was used to calculate the exact concentration of the compound.

UV-Vis absorption and fluorescence spectroscopy. UV-Visible absorption and fluorescence spectra were recorded on, respectively, UV mc² and FLX-Xenius XMF spectrophotometers from Safas, S.A., Monaco. The excitation wavelength was set at λ_{exc} = 420 nm for fluorescence experiments. 1 µL of a 2 mM stock solution in DMSO of cage/tetraconjugate was diluted with DMSO in a 1 cm Quartz cuvette to a final volume of 2 mL, reaching a final concentration of cage/tetra-conjugate of 1 µM. For the degradation study, either methoxy amine (final concentration: 100 mM) or 2-mercaptoethanol (final concentration: 5 mM) were added.

Dynamic light scattering and ζ potential. Particle size and ζ potential measurements were carried out on a Zetasizer Nano-ZS (Malvern, United Kingdom) using transparent ZEN0040 disposable cuvette (1000 µL) at 25 °C. The cages and conjugate compounds were prepared in deionized water at a final concentration of 1 µM. The measurements were performed immediately after the sample preparation.

General procedure for the synthesis of TPP Conjugates and TPP Cages. The protocol was adapted from previous reports.[52-54] **TPP-Ald**/**Zn-TPP-Ald** (1 eq., 80 µL of a 50 mM stock solution in DMSO) and peptide hydrazide (4 eq., 107 µL of a 150 mM stock solution in water) were mixed in 2 mL of DMSO, keeping the final concentration of the aldehyde building block at 2 mM with a final solvent composition of DMSO/H_2O 94/6. The reaction mixture was heated at 50 °C for 2 days, and product formation was monitored by LC-MS.

Singlet oxygen generation of TPP Conjugates and TPP Cages. Stock solutions of each TPP derivative at 0.02 mM and a stock solution of 9,10-anthracenediyl-bis(methylene)dimalonic acid (ABDA) at 2 mM were prepared in water. Solutions of 2 mL were prepared (final concentrations of TPP derivative and ABDA were 1 µM and 100 µM, respectively in 0.1 M phosphate buffer pH 7) in quartz cuvettes at room temperature. These solutions were submitted for one hour to visible green light irradiation (λ_{max} = 525 nm; 10 mW/cm², EvoluChem LED 525PF, HEPATOCHEM). The absorption decay of ABDA at 379 nm was measured every 3 minutes. Plots in $\ln(A_0/A)$ as a function of the elapsed irradiation time t in which A_0 and A are the ABDA absorbance at t = 0 and t, respectively. The dashed lines are linear least-squares fits to the respective data sets.

Cell culture. Human breast adenocarcinoma cell line (MCF-7) was maintained in Dulbecco's Modified Eagle Medium with nutrient mixture F12 (DMEM-F12) and supplemented with 10 % foetal bovine serum (FBS) and 1 % Penicillin/streptomycin (P/S). Cells were allowed to grow in humidified atmosphere at 37 °C under 5% CO_2.

Cell viability study. Cells were seeded in 96-well plate at a density of 5000 cells *per* well and left to incubate for 24 h. After incubation, cells were treated with different concentrations of compounds ranging from 0 to 20 µM. Cells treated with the vehicle were considered as control. After 3 days of incubation, 3-(4,5-dimethylthiazol-2-yl)-2,5-diphenyltetrazolium bromide (MTT) solution was added to cells at a final concentration of 0.5 mg mL^{-1} and cells were incubated for 4 h at 37°C. The viable cells have the ability to convert the yellow coloured water-soluble tetrazolium solution into purple coloured insoluble formazan crystals. After the end of incubation, the medium was aspirated and the crystals were dissolved in a mixture of ethanol and DMSO (1:1, v/v %) followed by 20 min shaking. The absorbance was measured using multiskan Sky (ThermoFisher scientific) at 540 nm and the percentage (%) of viable cells were calculated from the following equation: $Ab_{test}/Ab_{control}$ *100. The experiment was repeated three times.

Photodynamic therapy study. Cells were seeded in 96-well plate and left to grow for 24 h. Then, cells were treated with 1.31 µM concentration of the compounds and left to incubate for another 3 h or 24 h. After the end of incubation, cells were exposed to green light irradiation (λ_{exc} = 525 nm) using LED (EvoluChem LED 525PF, HEPATOCHEM, 10 mW/cm^2) for different times (5 min, 10 min, 15 min and 20 min). Cells kept in the dark were considered as non-irradiated controls. Twenty-four hours after irradiation, cell viability was evaluated using MTT assay as previously described. The experiment was repeated three times.

Reactive oxygen specifies (ROS) detection. Cells were seeded in 96-well plate and left to grow for 24 h. Then, cells were treated with 1.31 µM concentration of the compounds and left to incubate for another 24 h. After, incubation, ROS were detected using DCFDA/H2DCFDA-Cellular ROS Assay Kit (Abcam, UK) by incubating the cells with 20 µM of 2',7'-dichlorofluorescin diacetate (DCFDA) for 45 min at 37°C. Then, cells were exposed (or not) to green light irradiation for 2 min or 10 min. After irradiation, cells were washed once then visualized using EVOS-M5000 fluorescence microscope (ThermoFisher scientific) at λ_{ex}= 482/25 nm, objective 20x or 40x.

Uptake kinetics study using fluorescence activated cell sorting (FACS) assay. Cells were seeded in 12-well plate and left to grow for 24 h. After, cells were treated with 1.31 µM concentration of each compound and incubated for different time intervals (0.5 h, 1 h, 3 h, 6 h, 18 h and 24 h). After the end of incubation, cells were washed twice with phosphate buffered saline (PBS), trypsinized, then collected in culture medium and centrifuged for 5 min at 1300 rpm. The obtained cell pellets were suspended in DPBS containing $MgCl_2$ and $CaCl_2$ and cells kept in ice until the analyses. The flow cytometric analyses were performed using NovoCyte flow cytometer and the data were analyzed by NovoExpress software (ACEA Biosciences, Inc.). The evaluation of the internalization was carried out in 20 000 events. The experiment was repeated twice.

Imaging. Cells were seeded in glass bottom 8-well tissue culture chambers. Twenty-four hours after seeding, cells were treated with 2.62 µM **Cage-Arg** or **TPP-Arg$_4$** for 24 h. Hoechst 33342 was added at 10 µg mL^{-1} concentration for 20 min before the end of incubation. Then, cells were washed three times with culture medium and observed with LSM880 confocal microscope (Carl Zeiss, France) at 405 nm for Hoechst and 561 nm for compounds, phase contrast images were also acquired using a high magnification (63x/1.4 OIL Plan-Apo).

Endocytosis mechanism study. Cells were seeded in 12-well plate and left to grow for 24 h. After, cells were washed one time with PBS then incubated for 30 min with 5 mM of methyl-β-cyclodextrin, or 50 µM of chlorpromazine hydrochloride, or 40 µM of 5-(N,N-dimethyl) amiloride hydrochloride, or 1.2 mM of Ellman's Reagent (5,5-dithio-bis-(2-nitrobenzoic acid, DTNB) in FBS-free medium. Afterwards, cells were incubation with 1.31 µM of **Cage-Arg** in FBS-free medium containing inhibitors (or not) for 3 h. At the end of incubation, cells were prepared for FACS analysis as previously described. The experiment was repeated three times.

Dual therapy. Cells were seeded in 96-well plate and left to grow for 24 h. Then, cells were treated with 1.31 µM concentration of the compounds alone or with doxorubicin or with free doxorubicin (0.65 µM) and left to incubate for another 3 h. After the end of incubation, cells were exposed to green light irradiation (λ_{exc} = 525 nm) using LED (EvoluChem LED 525PF, HEPATOCHEM, 10 mW/cm^2)) for different times (2 min, 5 min, 10 min, 15 min and 20 min). Cells kept in the dark were considered as non-irradiated controls. Twenty-four after irradiation, cell viability was evaluated using MTT assay as previously described. The obtained combination effect was then investigated using CompuSyn software (ComboSyn, Inc). The experiment was repeated three times.

Conclusions

We reported the design and dynamic covalent self-assembly of porphyrin-peptide conjugates and cages through a hierarchical process involving the one-pot simultaneous formation of acylhydrazones and disulphides. The cages were shown to being chemically degradable and to form nanoparticles in aqueous media that effectively produce singlet oxygen upon green light irradiation. Cytotoxicity was absent in dark but was turned on upon green light irradiation. In particular, the non-metallated cationic cages **CAGE-Arg**, **CAGE-BA** and **CAGE-PPh$_3$** were found to display the best contrast – with low cytotoxicity in dark and good cytotoxicity upon light irradiation – and the fastest rate of cell uptake in the series. Finally, the combination with Doxorubicin was found to be synergistic, resulting in a potent dual cytotoxic effect. Overall, this study contributes to revealing the potential of novel organic nanostructures in PDT and dual therapies.

Author Contributions

CG: Investigation, Methodology; LMAA: Investigation; YB: Methodology; SC: Methodology; SR: Conceptualization, Funding acquisition, Supervision; NB: Conceptualization, Funding acquisition, Supervision; SU: Conceptualization, Funding acquisition, Project administration, Supervision, Writing original draft. The manuscript was written through contributions of all authors. All authors have reviewed/edited, and given approval to the final version of the manuscript.

Conflicts of interest

There are no conflicts to declare.

Acknowledgements

We thank MUSE, Université de Montpellier (ANR-16-IDEX-0006) for funding. We thank Dr. Emel Önal (Dogus University, İstanbul, Turkey) and Dr. Catherine Hirel (Sabanci University, İstanbul, Turkey) for an initial gift of **TPP-Ald**, Aurélien Lebrun for assistance with DOSY NMR, and Montpellier RIO Imaging

platform (ANR-10-INBS-04), member of France BioImaging, for imaging facilities and FACS analysis.

References

1. C. A. Robertson, D. H. Evans and H. Abraharnse, *J. Photochem. Photobiol. B, Biol.*, 2009, **96**, 1-8.
2. A. Juzeniene, Q. Peng and J. Moan, *Photochem. Photobiol. Sci.*, 2007, **6**, 1234-1245.
3. A. P. Castano, T. N. Demidova and M. R. Hamblin, *Photodiagn. Photodyn. Ther.*, 2005, **2**, 1-23.
4. M. R. H. Ana P. Castano Tatiana N. Demidova, *Photodiagnosis Photodyn. Ther.*, 2004, **1**, 279-293.
5. D. E. J. G. J. Dolmans, D. Fukumura and R. K. Jain, *Nat. Rev. Cancer*, 2003, **3**, 380-387.
6. T. Mishchenko, I. Balalaeva, A. Gorokhova, M. Vedunova and D. V. Krysko, *Cell Death Dis.*, 2022, **13**, 455.
7. N. L. Oleinick, R. L. Morris and T. Belichenko, *Photochem. Photobiol. Sci.*, 2002, **1**, 1-21.
8. M. Ethirajan, Y. H. Chen, P. Joshi and R. K. Pandey, *Chem. Soc. Rev.*, 2011, **40**, 340-362.
9. K. Szacilowski, W. Macyk, A. Drzewiecka-Matuszek, M. Brindell and G. Stochel, *Chem. Rev.*, 2005, **105**, 2647-2694.
10. A. P. Castano, T. N. Demidova and M. R. Hamblin, *Photodiagn. Photodyn. Ther.*, 2004, **1**, 279-293.
11. T. C. Pham, V. N. Nguyen, Y. Choi, S. Lee and J. Yoon, *Chem. Rev.*, 2021, **121**, 13454-13619.
12. Y. F. Kang, W. K. Chen, K. X. Teng, L. Y. Wang, X. C. Xu, L. Y. Niu, G. Cui and Q. Z. Yang, *CCS Chem.*, 2022, **4**, 3516-3528.
13. F. Hu, S. Xu and B. Liu, *Adv. Mater.*, 2018, **30**, e1801350.
14. F. Ricchelli, *J. Photochem. Photobiol. B, Biol.*, 1995, **29**, 109-118.
15. Y. C. Liu, G. J. Liu, W. Zhou, G. L. Feng, Q. Y. Ma, Y. Zhang and G. W. Xing, *Angew. Chem. Int. Ed.*, 2023, DOI: 10.1002/anie.202309786, e202309786.
16. V. Almeida-Marrero, M. Mascaraque, M. J. Vicente-Arana, A. Juarranz, T. Torres and A. de la Escosura, *Chem. Eur. J.*, 2021, **27**, 9634-9642.
17. I. Sehgal, M. Sibrian-Vazquez and M. G. H. Vicente, *J. Med. Chem.*, 2008, **51**, 6014-6020.
18. M. Sibrian-Vazquez, T. J. Jensen, R. P. Hammer and M. G. H. Vicente, *J. Med. Chem.*, 2006, **49**, 1364-1372.
19. V. Almeida-Marrero, F. Bethlehem, S. Longo, M. C. Bertolino, T. Torres, J. Huskens and A. de la Escosura, *Angew. Chem. Int. Ed.*, 2022, **61**, e202206900.
20. L. M. A. Ali, K. Miyagawa, N. Fukui, M. Onofre, K. El Cheikh, A. Morere, S. Clement, M. Gary-Bobo, S. Richeter and H. Shinokubo, *Org. Biomol. Chem.*, 2022, **20**, 8217-8222.
21. R. Wang, X. S. Li and J. Yoon, *Acs Appl Mater Inter*, 2021, **13**, 19543-19571.
22. C. L. Conway, I. Walker, A. Bell, D. J. H. Roberts, S. B. Brown and D. I. Vernon, *Photochem. Photobiol. Sci.*, 2008, **7**, 290-298.
23. M. Boisbrun, R. Vanderesse, P. Engrand, A. Olie, S. Hupont, J. B. Regnouf-De-Vains and C. Frochot, *Tetrahedron*, 2008, **64**, 3494-3504.
24. C. Frochot, B. Di Stasio, R. Vanderesse, M. J. Belgy, M. Dodeller, F. Guillemin, M. L. Viriot and M. Barberi-Heyob, *Bioorg. Chem.*, 2007, **35**, 205-220.
25. L. Tirand, C. Frochot, R. Vanderesse, N. Thornas, E. Trinquet, S. Pinel, M. L. Viriot, F. Guillemin and M. Barberi-Heyob, *J. Control. Release*, 2006, **111**, 153-164.
26. M. K. Kuimova, G. Yahioglu and P. R. Ogilby, *J. Am. Chem. Soc.*, 2009, **131**, 332-340.
27. E. Clo, J. W. Snyder, P. R. Ogilby and K. V. Gothelf, *Chembiochem*, 2007, **8**, 475-481.
28. S. Hatz, J. D. C. Lambert and P. R. Ogilby, *Photochem. Photobiol. Sci.*, 2007, **6**, 1106-1116.
29. B. B. Sun, R. Chang, S. P. Cao, C. Q. Yuan, L. Y. Zhao, H. W. Yang, J. B. Li, X. H. Yan and J. C. M. van Hest, *Angew. Chem. Int. Ed.*, 2020, **59**, 20582-20588.
30. F. Biscaglia and M. Gobbo, *Peptide Sci.*, 2018, **110**, e24038.
31. Q. L. Zou, M. Abbas, L. Y. Zhao, S. K. Li, G. Z. Shen and X. H. Yan, *J. Am. Chem. Soc.*, 2017, **139**, 1921-1927.
32. Y. Wu, H. F. Chau, Y. H. Yeung, W. Thor, H. Y. Kai, W. L. Chan and K. L. Wong, *Angew. Chem. Int. Ed.*, 2022, **61**, e202207532.
33. X. L. Zheng, S. N. Lei, Z. K. Gao, X. Y. Dong, H. Y. Xiao, W. M. Liu, C. H. Tung, L. Z. Wu, P. F. Wang and H. Cong, *Chem. Sci.*, 2023, **14**, 3523-3530.
34. L. Xia, J. Wu, B. X. Huang, Y. Gao, J. Tian and W. A. Zhang, *Chem. Commun.*, 2020, **56**, 11134-11137.
35. L. Shao, Y. T. Pan, B. Hua, S. D. Xu, G. C. Yu, M. B. Wang, B. Liu and F. H. Huang, *Angew. Chem. Int. Ed.*, 2020, **59**, 11779-11783.
36. I. Roy, S. Bobbala, R. M. Young, Y. Beldjoudi, M. T. Nguyen, M. M. Cetin, J. A. Cooper, S. Allen, O. Anamimoghadam, E. A. Scott, M. R. Wasielewski and J. F. Stoddart, *J. Am. Chem. Soc.*, 2019, **141**, 12296-12304.
37. H. T. Z. Zhu, H. H. Wang, B. B. Shi, L. Q. Shangguan, W. J. Tong, G. C. Yu, Z. W. Mao and F. H. Huang, *Nat. Commun.*, 2019, **10**, 2412.
38. X. Jiang, Z. X. Zhou, H. Yang, C. Shan, H. Yu, L. Wojtas, M. M. Zhang, Z. W. Mao, M. Wang and P. J. Stang, *Inorg Chem*, 2020, **59**, 7380-7388.
39. G. C. Yu, S. Yu, M. L. Saha, J. Zhou, T. R. Cook, B. C. Yung, J. Chen, Z. W. Mao, F. W. Zhang, Z. J. Zhou, Y. J. Liu, L. Shao, S. Wang, C. Y. Gao, F. H. Huang, P. J. Stang and X. Y. Chen, *Nat. Commun.*, 2018, **9**, 4335.
40. W. Y. Li, J. J. Wan, J. L. Kan, B. Wang, T. Song, Q. Guan, L. L. Zhou, Y. A. Li and Y. B. Dong, *Chem. Sci.*, 2023, **14**, 1453-1460.
41. J. F. Lovell, C. S. Jin, E. Huynh, H. L. Jin, C. Kim, J. L. Rubinstein, W. C. W. Chan, W. G. Cao, L. V. Wang and G. Zheng, *Nat. Mater.*, 2011, **10**, 324-332.
42. B. B. Sun, X. P. Guo, M. Feng, S. P. Cao, H. W. Yang, H. L. Wu, M. H. M. E. van Stevendaal, R. A. J. F. Oerlemans, J. N. Liang, Y. Q. Ouyang and J. C. M. van Hest, *Angew. Chem. Int. Ed.*, 2022, **61**, e202208732.
43. L. L. Zhao, Y. L. Xing, R. Wang, F. F. Yu and F. B. Yu, *ACS Appl. Bio. Mater.*, 2020, **3**, 86-106.
44. F. Lu, H. W. Zhang, W. Pan, N. Li and B. Tang, *Chem. Commun.*, 2021, **57**, 7067-7082.
45. S. Ulrich, *Acc. Chem. Res.*, 2019, **52**, 510-519.
46. J. F. Reuther, J. L. Dees, I. V. Kolesnichenko, E. T. Hernandez, D. V. Ukraintsev, R. Guduru, M. Whiteley and E. V. Anslyn, *Nat. Chem.*, 2018, **10**, 45-50.
47. D. Al Kelabi, A. Dey, L. O. Alimi, H. Piwonski, S. Habuchi and N. M. Khashab, *Chem. Sci.*, 2022, **13**, 7341-7346.
48. Y. Kim, J. Koo, I. C. Hwang, R. D. Mukhopadhyay, S. Hong, J. Yoo, A. A. Dar, I. Kim, D. Moon, T. J. Shin, Y. H. Ko and K. Kim, *J. Am. Chem. Soc.*, 2018, **140**, 14547-14551.
49. G. Q. Lin, H. M. Ding, R. F. Chen, Z. K. Peng, B. S. Wang and C. Wang, *J. Am. Chem. Soc.*, 2017, **139**, 8705-8709.
50. C. Pavani, A. F. Uchoa, C. S. Oliveira, Y. Iamamoto and M. S. Baptista, *Photochem. Photobiol. Sci.*, 2009, **8**, 233-240.
51. S. Durot, J. Taesch and V. Heitz, *Chem. Rev.*, 2014, **114**, 8542-8578.

52. E. Suárez-Picado, M. Coste, J.-Y. Runser, M. Fossépré, A. Carvalho, M. Surin, L. Jierry and S. Ulrich, *Biomacromolecules*, 2022, **23**, 431-442.
53. M. Konopka, P. Cecot, S. Ulrich and A. R. Stefankiewicz, *Front. Chem.*, 2019, **7**, 503.
54. W. Drozdz, C. Bouillon, C. Kotras, S. Richeter, M. Barboiu, S. Clément, A. R. Stefankiewicz and S. Ulrich, *Chem. Eur. J.*, 2017, **23**, 18010-18018.
55. Q. Laurent, R. Martinent, B. Lim, A. T. Pham, T. Kato, J. Lopez-Andarias, N. Sakai and S. Matile, *JACS Au*, 2021, **1**, 710-728.
56. G. Gasparini, E. K. Bang, G. Molinard, D. V. Tulumello, S. Ward, S. O. Kelley, A. Roux, N. Sakai and S. Matile, *J. Am. Chem. Soc.*, 2014, **136**, 6069-6074.
57. D. Kalafatovic and E. Giralt, *Molecules*, 2017, **22**, 1929.
58. C. Bechara and S. Sagan, *Febs Letters*, 2013, **587**, 1693-1702.
59. R. N. Wang, C. F. Yin, C. R. Liu, Y. Sun, P. P. Xiao, J. Li, S. Yang, W. Wu and X. Q. Jiang, *J. Am. Chem. Soc.*, 2021, **143**, 20927-20938.
60. M. Y. Shao, Y. Qi, D. D. Sui and F. J. Xu, *Biomater Sci-Uk*, 2021, **9**, 7104-7114.
61. X. Y. Zhang, D. S. Alves, J. C. Lou, S. D. Hill, F. N. Barrera and M. D. Best, *Chem. Commun.*, 2018, **54**, 6169-6172.
62. G. A. Ellis, M. J. Palte and R. T. Raines, *J. Am. Chem. Soc.*, 2012, **134**, 3631-3634.
63. S. M. Mahalingam, J. D. Ordaz and P. S. Low, *Acs Omega*, 2018, **3**, 6066-6074.
64. M. T. Jeena, L. Palanikumar, E. M. Go, I. Kim, M. G. Kang, S. Lee, S. Park, H. Choi, C. Kim, S. M. Jin, S. C. Bae, H. W. Rhee, E. Lee, S. K. Kwak and J. H. Ryu, *Nat. Commun.*, 2017, **8**, 26.
65. W. Lv, Z. Zhang, K. Y. Zhang, H. R. Yang, S. J. Liu, A. Q. Xu, S. Guo, Q. Zhao and W. Huang, *Angew. Chem. Int. Ed.*, 2016, **55**, 9947-9951.
66. E. Onal, V. Ahsen, J. Pecaut, D. Luneau and C. Hirel, *Tetrahedron Lett.*, 2015, **56**, 5157-5160.
67. Broad peaks were often observed, which we assign to multiple acylhydrazone/disulphide configurational/conformational isomers being formed (see reference 54).
68. M. Merchat, G. Bertolini, P. Giacomini, A. Villanueva and G. Jori, *J. Photochem. Photobiol. B, Biol.*, 1996, **32**, 153-157.
69. H. Q. Cao, Y. F. Qi, X. B. Gao, J. W. Zi, J. R. Xia, L. Wang, H. Wang, Y. Yang and J. B. Li, *Chem. Commun.*, 2021, **57**, 2245-2248.
70. I. A. Khalil, K. Kogure, H. Akita and H. Harashima, *Pharmacol Rev*, 2006, **58**, 32-45.
71. N. Kwon, H. Kim, X. S. Li and J. Yoon, *Chem. Sci.*, 2021, **12**, 7248-7268.
72. K. Berg, A. Weyergang, L. Prasmickaite, A. Bonsted, A. Hogset, M. T. R. Strand, E. Wagner and P. K. Selbo, in *Photodynamic Therapy. Methods in Molecular Biology*, ed. C. Gomer, Humana Press, Totowa, NJ, 2010, vol. 635, pp. 133-145.
73. K. Berg, P. K. Selbo, L. Prasmickaite, T. E. Tjelle, K. Sandvig, D. Moan, G. Gaudernack, O. Fodstad, S. Kjolsrud, H. Anholt, G. H. Rodal, S. K. Rodal and A. Hogset, *Cancer Res*, 1999, **59**, 1180-1183.
74. M. Ahmed and A. A. A. Hashim, *Res. Chem. Intermed.*, 2016, **42**, 1777-1789.
75. L. Panasci, B. J. JeanClaude, D. Vasilescu, A. Mustafa, S. Damian, Z. Damian, E. Georges, Z. Liu, G. Batist and B. LeylandJones, *Biochem Pharmacol*, 1996, **52**, 1097-1102.
76. E. Bartolami, Y. Bessin, N. Bettache, M. Gary-Bobo, M. Garcia, P. Dumy and S. Ulrich, *Org. Biomol. Chem.*, 2015, **13**, 9427-9438.